Application of the END Theory to the $H + D_2 \rightarrow HD + D$ Reaction†

R. Cabrera-Trujillo, Y. Öhrn,* E. Deumens, and J. R. Sabin

Quantum Theory Project, Departments of Physics and Chemistry, University of Florida, Gainesville, Florida 32611-8435

Received: March 15, 2004; In Final Form: April 12, 2004

We investigate time-delay effects in the formation of HD products when H projectiles collide with D_2 targets with a collision energy of 1.64 eV in the center-of-mass frame using the electron−nuclear dynamics (END) approach. Trajectories having target orientations within a 60° cone measured about the D−D bond are those that lead to the production of HD. In the impact-parameter regions that correspond to the formation of HD, we note a large change in the scattering angle of the HD product within a localized narrow region as a function of impact parameter. Calculated classical and semiclassical differential reaction cross sections are presented and compared to available experimental data. Finally, a coherent-state study of the vibrational modes for the product HD is presented.

1. Introduction

Scattering resonances in chemical reactions were the topic of discussion in the theory of molecular reaction dynamics in the 1970s[1−3] for collinear $H + H_2$ collisions. The $H + H_2$ reaction was later studied in three dimensions.[4] Experimental results showing resonant behavior in the integral cross section of the hydrogen exchange reaction were reported around 1990[5,6] but were in contradiction with theoretical[7,8] and other experimental[9] work. This latter work showed that, although resonances were not observed in the integral cross section, it was suggested at the time that they should be detectable in the energy dependence of the state-resolved differential cross sections[10,11] for the $H + H_2$ and $D + H_2$ reactions. Experimental work and theoretical quantum mechanical calculations on a ground-state potential surface for the $H + HD \rightarrow D + H_2$ reaction[12] show a slowing of the intermediate in the forward scattering, which is interpreted as a "quantized bottleneck state" at the top of the barrier.

Over the past several years, fully state-resolved differential cross sections for the $H + D_2$ reaction have been measured.[13−19] Attempts to find signatures of resonances for this system for collision energies around 1.25 eV in the center-of-mass frame by experiment and theory have failed.[20,21]

In a very interesting communication[23] reporting time-of-flight measurements and quasi-classical trajectory (QCT) calculations using the BKMP2 potential energy surface,[24] evidence was presented for a time-delay behavior between backward- and forward-scattered products in the $H + D_2 \rightarrow HD + D$ reaction at 1.64 ± 0.05 eV. The most prominent evidence for the existence of resonance in this reaction is the observation of a time delay, estimated to be about 25 fs between the backward- and forward-scattered product HD molecules. The delay between the formation of the products in the backward and forward directions is discussed in a time-dependent quantum mechanical study using the same potential surface in a recent letter to *Nature*.[25] The time delay is estimated to be about 25 fs. Comparisons to time-of-flight measurements made on the nanosocond time scale are attempted.

In this paper we revisit this canonical exchange problem using electron nuclear dynamics (END)[26,27] to study the details of the time evolution of the reaction $H + D_2 \rightarrow HD + D$ at 1.64 eV (in the center-of-mass frame). In the next section, we give a brief account of minimal END theory, which is a time-dependent, direct, and nonadibatic approach to molecular reaction dynamics. This is followed by sections presenting and discussing the calculations and results.

It is fitting to contribute this paper to this memorial issue of *J. Phys. Chem. A* for Gert Due Billing. During the development of END, one of us (Y.Ö.) visited H. C. Ørsted Institute on a number of occasions and remembers Gert's challenge to apply the minimal END theory to neutral reactants at lower energies. In his memory, we apply his suggestion in this contribution.

2. Theory

Electron nuclear dynamics[27] is a time-dependent theory of molecular processes that can be characterized as a direct, nonadiabatic approach. Starting from a given form of the wave function for all electrons and atomic nuclei of the system, the quantum mechanical action is formed and made stationary, producing an approximation to the time-dependent Schrödinger equation for the total reacting system. This approximation takes the form of a set of coupled first-order differential equations in the time variable. The wave-function parameters, which carry the time dependence, can be complex and are the dynamical variables of the system. Their time evolution is governed by the END equations.[26,27]

The choice of system wave function, including the basis in which it is expressed, defines the level of approximation to the END equations. The minimal implementation of END consist of classical nuclei, or nuclei in the narrow-width Gaussian wave-packet limit, with average positions **R** and momenta **P** and of electrons described by a spin-unrestricted single determinant[28] of spin orbitals

$$\chi_h = u_h + \sum_{p=N+1}^{K} u_p z_{ph}, \quad h = 1, 2, ..., N \tag{1}$$

expressed in terms of a basis of atomic functions, u_{i1}^K, centered

† Part of the "Gert D. Billing Memorial Issue".

* To whom correspondence should be addressed. E-mail: ohrn@qtp.ufl.edu.

10.1021/jp0488517 CCC: $27.50
Published on Web 05/21/2004

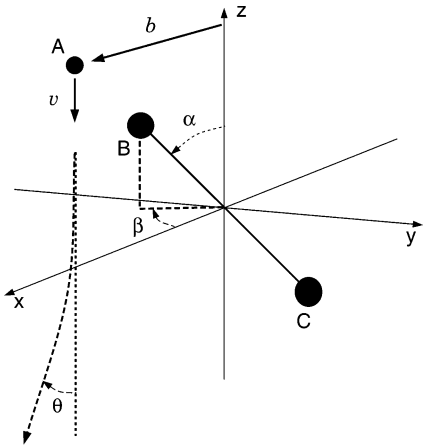

Figure 1. Schematic representation of the initial conditions of the projectile−target system as required by the END formalism. Projectile moving in the negative *z* direction.

on the average nuclear positions and moving with the nuclei. The dynamics takes place in a Cartesian laboratory system. Thus, the dynamical variables in minimal END are the Cartesian components of nuclear positions and momenta, and the complex molecular orbital coefficients z_{ph}. The nonadiabatic couplings are treated explicitly, and the overall translational and rotational degrees of freedom are not separated from the internal dynamics. However, because the fundamental conservation laws for total linear and angular momentum hold, transformation to internal or center-of-mass coordinates is possible at any stage of the dynamics.

The treatment of the dynamics of all electrons and nuclei simultaneously means that the END equations contain two different time scales. Integration of the equations must be able to handle both of them, as well as the demanding molecular integral computations at each time step. The ENDyne code[29] is able to do that in an efficient manner. This code, which implements minimal END, has been applied to a number of reactive collisions involving ions, atoms, and molecules. Differential and integral cross sections and other details of the reaction dynamics are found to be in agreement with the best experiments, in particular for collision energies well above thermal energy.[30−37] The success of minimal END in predicting reliable cross sections for reactive processes at energies from a few electronvolts to tens of kiloelectronvolts makes it interesting to push this level of theory to lower energies and to consider problems which have been studied in great detail by both experiment and theory. With this in mind, we apply minimal END to the reaction $H + D_2 \rightarrow HD + D$. The results are discussed in the next section.

3. Calculations and Results

3.1. Initial Conditions. The time-dependent analysis of the collision within the END approach requires the specification of initial conditions of the system under consideration. Figure 1 shows a schematic representation of the $H \rightarrow D_2$ arrangement. In the case of atomic projectiles, as in this case, we need to consider the initial orientations only of the target. The target center of mass is initially placed at the origin of a Cartesian laboratory coordinate system, and its orientation is specified by the angles α and β. For this system, we consider an orientation grid with steps of 20° in the angles α and β. This generates a grid of 164 orientations of which 50 are independent, i.e., are not related via symmetry.

The molecular target, D_2, is initially in its $^1\Sigma_g^+$ electronic ground state for the equilibrium geometry as computed in the computational basis at the SCF level. The basis functions used for the atomic orbital expansion are derived from those optimized by Dunning.[38,39] The atomic bases consist of a 5s2p/5s2p set with the addition of an even-tempered diffuse s and p orbitals for a better description of the long-range interaction.

We perform the rotational average of a target property, *g*, as described in ref 40. That is

$$\bar{g} = \frac{1}{4\pi}\int g(\alpha,\beta)\,\sin\beta\,d\beta\,d\alpha \tag{2}$$

where $g(\alpha,\beta)$ is the property of interest. The trapezoidal rule with $h = 2\pi/n$ is used for the α integrations, such that

$$\frac{1}{2\pi}\int_0^{2\pi} f(\alpha)\,d\alpha = \frac{h}{2\pi}\sum_{j=0}^{m-1} f_j \tag{3}$$

The average over β is approximated by applying the trapezoidal rule to the function $f(\beta)$ leaving the weight function $\sin\beta$ to be integrated explicitly. Thus

$$\frac{1}{2}\int_0^{\pi} f(\beta)\sin\beta\,d\beta = \frac{1}{2}\sum_{i=0}^{n-1}\int_{\beta_i}^{\beta_{i+1}} \tilde{f}_i(\beta)\sin\beta\,d\beta = \frac{1}{2}\sum_{i=0}^{n-1}\bar{f}_i \tag{4}$$

with

$$\tilde{f}_i(\beta) = f_i + \frac{\beta-\beta_i}{\beta_{i+1}-\beta_i}(f_{i+1}-f_i) \tag{5}$$

After integration using this numerical grid, one obtains

$$\bar{f}_i = f_i\left(\cos\beta_i - \frac{\sin\beta_{i+1}-\sin\beta_i}{\beta_{i+1}-\beta_i}\right) + f_{i+1}\left(\frac{\sin\beta_{i+1}-\sin\beta_i}{\beta_{i+1}-\beta_i} - \cos\beta_{i+1}\right) \tag{6}$$

The projectile is set initially at a distance of 20.0 au from the target along the *z* axis and with an impact parameter of *b*, as shown in Figure 1. The initial projectile velocity is set parallel to the *z* axis and directed toward the stationary target. The trajectory evolves until the projectile is 20 au past the target or until there are no longer changes in the energy, velocity, or charge of the projectile. We consider values of the impact parameter from 0.0 to 15.0 au, which we separate into three regions. For close collisions, from 0.0 to 6.0 au, we use steps of 0.1 au. For the intermediate region, from 6.0 to 10.0 au, we use steps of 0.5 au, and for $b > 10.0$, we use steps of 1.0. This give us 74 fully dynamical trajectories for each target orientation and projectile energy. Once we have identified the impact-parameter region where the reaction occurs, we refine the numerical impact-parameter grid until we obtain a smooth deflection function (vide infra). Thus, at the end of each trajectory, one obtains the total wave function and the nuclear positions and momenta. Therefore, one is able to calculate the deflection function, $\Theta(b)$, and electronic properties, e.g., charge transfer and energy loss, as well as the rovibrational properties of the molecular products of interest.

4. Potential Energy Surface

The projectile experiences a head-on collision with one of the D atoms for impact-parameter values in the range of $0 < b < D/2$, where *D* is the D_2 bond distance, the exact value

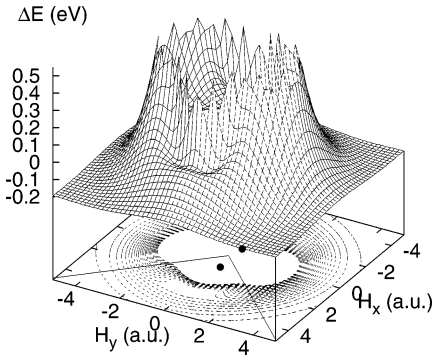

Figure 2. Potential energy surface for a rigid D_2 molecule with a bond length corresponding to the outer classical turning point and with the hydrogen atom placed at (H_x, H_y). The displayed local minimum at (3.0, 0) in a 60° cone (diagonal lines in the *xy* plane to guide the eye) about the D_2 bond length is the region that corresponds to the formation of HD.

depending on the initial target orientation. Animation of such trajectories that lead to reaction shows that the D_2 bond stretches as the *H* atom approaches and the three particles spend some brief time together before the HD bond is fully formed and the products separate.

Using a fixed D_2 bond length corresponding to the outer classical turning point for the first vibrational state, calculating the electronic energy of H + D_2, and subtracting the ground-state electronic energy of the separated H atom and D_2 molecule, we can construct a potential energy surface as a function of the position, (H_x, H_y), of the *H* atom. A graph of this function is shown in Figure 2. We note that the incoming hydrogen atom encounters a small potential energy well in a narrow region forming a cone about the D−D bond with an angle of 45° from the D−D axis. When a trajectory is such that the incoming hydrogen arrives inside this cone, we observe the exchange of one of the D atoms with the incoming hydrogen to produce HD. However, this explanation is based on potential surface analysis with the D−D fixed bond distance. From the fully dynamical trajectories, we observe that the reaction occurs up to orientational angles of 60°, or within a conical angle of 120°. The expansion of the D_2 bond is responsible for the exchange with the incoming hydrogen atom. The question then arises whether this small potential well is strong enough to hold the three particles together long enough to form a HD_2 "complex". This we address next.

4.1. Deflection Function. From the set of trajectories that result in the product HD, we calculate the scattering angle in the center-of-mass frame with respect to the incoming direction of the hydrogen atom. Thus, products that move with a scattering angle of less than 90° are moving forward. The scattering angle as a function of the impact parameter determines the deflection function for the collision. The deflection function is the critical ingredient in computations of the classical and semiclassical differential cross sections. Because of the complexity of this system, the deflection functions require some analysis before we can move to the differential cross section.

In Figure 3, we show the deflection function, in the center-of-mass frame, of the collision for the target orientations β = 0° and β = 180° and α = 0°, 20°, 40°, 60° as a function of impact parameter *b*. The orientations for β = 180° are shown on the negative *b*-axis. It is interesting to note that the reaction occurs in general for a finite range of impact parameters with a very sharp cut off on both ends of the range. Most of the ranges show a predominance of backscattering and a relatively small range of impact parameters with forward scattering. The

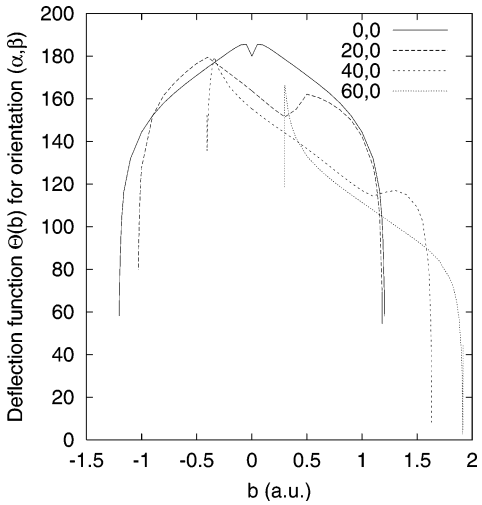

Figure 3. Deflection function for the target orientations (β = 0; α = 0, 20, 40, 60°) for formation of HD in the collision H + D_2 → HD + D as a function of the impact parameter from b = −2 to b = 2, which is the same as β = 0° and β = 180°. This figure shows the structure of the glory and rainbow angles.

graphs for β = 20°, 40°, and 60° are qualitatively similar. There is no reaction for α > 60°.

The classical cross sections exhibit singularities when the deflection function has a zero derivative, which causes rainbow scattering, and when the deflection function goes through zero, which causes glory scattering. In Figure 3, we note that the deflection function for each α value has two or three extrema points with zero derivative. The deflection function for α = 0° has extrema for b = 0.1 and ±0.05 (rainbow) and has zeroes for b = ±0.3 (glory) and for b = 0. When α increases, the two glory values turn into rainbow angles. As a result, there is a continuous family of multiple rainbow angles, which means that the differential cross section averaged over orientation has a continuous sequence of singularities from θ = 180° to θ = 115°.

4.2. Reaction Differential Cross Section. From the deflection function for the HD product channel, we obtain the reaction differential cross section. In previous works, we have implemented the Schiff approximation[41] for the analysis of differential cross sections for collisions in the medium- to high-energy regions.[32−36] We now apply the Schiff approximation at lower energy to obtain a semiclassical correction to the classical differential cross section for the HD product channel. The Schiff approximation is valid for kR > 1, where k is the wave vector of the projectile and R is the potential range. Because $k \approx 15.0$ au and we have a long-range interaction, we are within the applicability range of the Schiff approximation.

In Figure 4, we show the orientationally averaged differential cross section for the formation of HD as a function of the scattering angle in the center-of-mass frame. In the same figure, we compare our results to the experimental data of refs 42 and 43 for a collision energy of 1.29 eV in the center-of-mass frame. Even though there is, for each orientation, a minimal impact parameter for which there is a reaction, the average differential cross section is nonzero for all θ up to 180°. The classical DCS is not shown above 150° because that region is a continuum of singularities. The Schiff approximation is applied to the classical differential cross section for each orientation, and the resulting DCS is averaged. From these results, we observe that the Schiff approximation follows the classical results closely and corrects for the rainbow and backward peak character of the scattering.

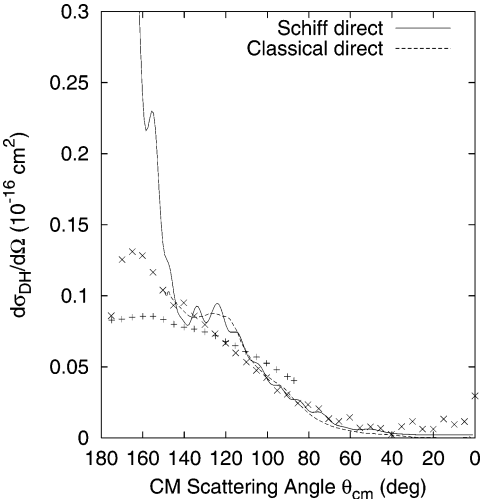

Figure 4. Differential cross section for the formation of HD in the collision H + D_2 → HD + D as a function of the scattering angle in the center-of-mass frame. The solid line is the semiclassical result using the Schiff approximation (see text). The dashed line is the classical differential cross section; it is not shown for angles larger than 150° because that region is a continuum of singularities. The experimental work at 1.29 eV is from (×) ref 42 and (+) ref 43.

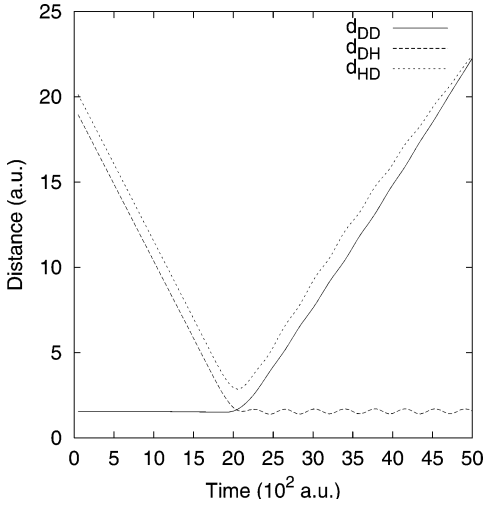

Figure 5. Backward scattering: Interparticle distances for target orientation $\alpha = 40°$ and $\beta = 0°$ and impact parameter $b = 0$. This trajectory illustrates a quick bounce back to produce backward scattering.

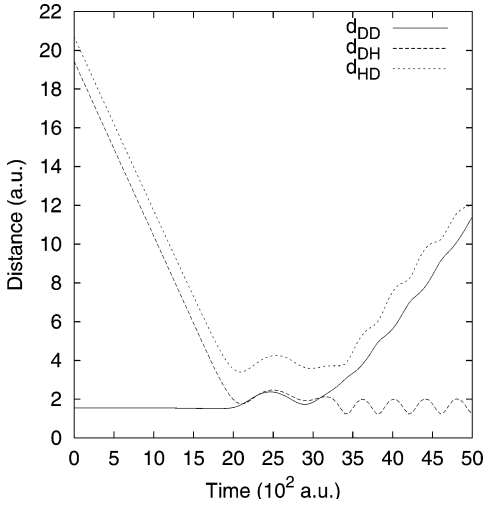

Figure 6. Forward scattering: Interparticle distances for target orientation $\alpha = 40°$ and $\beta = 0°$ and impact parameter $b = 1.6304$. This trajectory illustrates a more involved process where the projectile and target spend a slightly longer time together, enough for the H to rotate around so that the DH leaves in the forward direction.

It transforms the classical DCS with its continuum of infinite values into a finite DCS.

There is rather good agreement of both classical and quantum treatments with the experimental work of Kitsopoulos et al.[42] for the angular scattering region of 120−0°. The large discrepancy for backward scattering between the Schiff approximation and the experimental results is the result of the fact that the Schiff approximation provides semiclassical corrections only within the scattering process for each orientation and then the results are averaged. Quantum interference between trajectories from different orientations is responsible for the difference between the theoretical DCS shown in Figure 4 and the experimental values. We are not aware of a semiclassical method that will treat all trajectories scattering off multiple orientations of a nonspherical target.

4.3. Time Delay. In the study of the H + D_2 reaction, two notions of time delay are relevant. Unfortunatley, not all authors make a clear distinction between the two. In this section, we discuss the notion of time delay as defined in the formal theory of scattering. It is the delay that could be observed in principle between the products that scatter directly and those that go through a long-lived state. The second notion of time delay sometimes used in H + D_2 studies is a reflection of the fact that some products leave the reaction with a higher velocity. That notion will be discussed in the next section.

Fernández-Alonso and Zare[16] discussed the time delay obtained from a quasi-classical trajectory calculation. In Figures 5 and 6, we show two trajectories that illustrate the time that the forward-scattered HD is delayed with respect to the backward-scattered HD. The forward-scatteredback trajectory lingers about 15 fs as a three-particle complex before the D and HD separate. The backward-scattered trajectory shows that the HD leaves immediately. Also note that the departing velocity of the backward-scattered HD is slightly higher, has a steeper slope in Figure 5, than the velocity of the forward-scattered HD in Figure 6.

Kliner and collaborators[25] show the result of a quantum wave packet calculation where the forward-scattered fraction of the wave packet is delayed by about 25 fs in relation to the backward-scattered part of the wave packet. This can be verifyed within the END results from Figures 5 and 6. In Figure 5, the HD product leaves a perimeter of $R = 3.0$ au at a time $t \approx 2400$ au for the backward scattering; meanwhile, $t \approx 3400$ au for the forward scattering (Figure 6). This gives a delay of ∼1000 au or ∼24.0 fs.

4.4. Velocity Distribution. In addition to the products lingering a different amount of time in the interaction region and some of them forming a short-lived three-particle complex, the H + D_2 → DH + D reaction shows a significant angular dependence of asymptotic velocity. From the differential cross section, we note that the majority of the particles are scattered backward. However, a small portion of the incident beam is scattered forward. Time-of-flight experiments[25] show a time delay of 25 fs between the forward- and backward-scattered products; the majority are backward-scattered and arrive at the detector first. To quantify the difference in velocity, we compute the orientational average as a function of scattering angle. In line with previous authors, we present that data as a time $\tau = 3/v$. The distance of 3 au is chosen to follow previous theoretical analysis.[25]

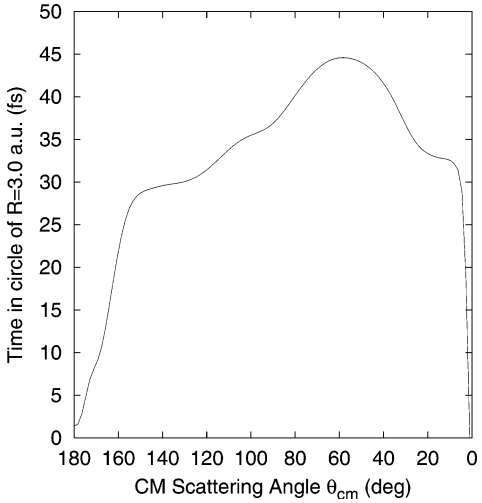

Figure 7. Time required for HD to traverse a distance of $R = 3.0$ au with asymptotic velocity in the collision H + D_2 → HD + D as a function of the center-of-mass scattering angle.

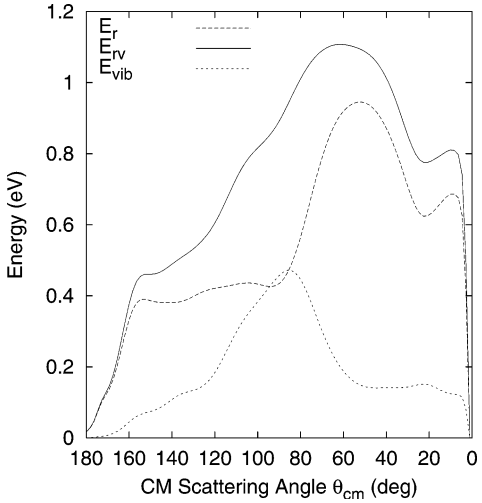

Figure 8. Rovibrational, E_{rv}; vibrational, E_{vib}; and rotational, E_r, energies for the product HD in the collision H + D_2 → HD + D as a function of the scattering angle in the center-of-mass frame.

Because, for each target orientation, we obtain a differential reaction cross section that is proportional to the number of particles scattered within a solid angle $d\Omega(\theta,\varphi)$, we average over all target orientations. We construct a differential-cross-section-weighted average for a property $h(\theta)$ via

$$\bar{h}(\theta) = \frac{\int h(\theta,\alpha,\beta)\,\frac{d\sigma(\theta,\alpha,\beta)}{d\Omega}\sin\beta\, d\beta\, d\alpha}{\int \frac{d\sigma(\theta,\alpha,\beta)}{d\Omega}\sin\beta\, d\beta\, d\alpha} \qquad (7)$$

In Figure 7, we show the time required for a particle to travel the distance $R = 3.0$ au in the center-of-mass frame. First, we observe that particles scattered in the forward direction ($0° < \theta < 90°$) take longer to travel than those that travel backward ($90° < \theta < 180°$). The average difference is the time delay caused by the velocity inhomogeneity. Thus, for example, the slowest trajectories around $\theta_{cm} \approx 60°$ when compared to $\theta_{cm} \approx 140°$ have a delay of 15 fs. However, if we take the slowest and fastest particles produced by the dynamics, without weighting with the differential cross section, we calculate a time delay of 23.0 fs, in agreement with previoulys reported time delays determined by quantum scattering calculations on a ground-state surface.[25]

Because of the large value of the theoretical differential cross section for backward scattering (see Figure 4), trajectories with no time delay dominate the average near 180°. As a result, the time delay in Figure 7 becomes too small near 180°.

4.5. Vibrational and Rotational Analysis. The velocity distribution allows one to understand the correlation between the vibrational excitation of the products and the angle of scattering (forward or backward). To perform a vibrational study of the HD products at the end of each trajectory, we separate the rotational and vibrational energies.

In Figure 8, we show the results for the rovibrational, rotational, and vibrational energies of the product HD as a function of the scattering in the center-of-mass frame of the collision, obtained by the same procedure as the time delay, i.e., by averaging over the target orientations. First, it is interesting to note that the slow, forward-scattered products are the ones with the highest rovibrational energy. This is in accordance with conservation of energy, as in this case, the translational energy has been converted into rotations and/or vibrations. The translational energy $E_t \sim v^2 \sim (1/t)^2$, from the results in Figure 7, is low for $20° < \theta_{cm} < 100°$, corresponding to the forward scattering. Furthermore, the HD products scattered perpendicular to the incoming projectile direction have the highest vibrational energy.

To decompose the vibrational state of the HD product, we make use of the vibrational coherent-state representation.[44] Each product is described by the evolving state

$$|\lambda\rangle = e^{-(1/2)|\lambda|^2}\sum_n \frac{\lambda^n}{\sqrt{n!}}|n\rangle \qquad (8)$$

in terms of the harmonic oscillator eigenstates $|n\rangle$ for the normal modes. Here, λ is a time-dependent complex parameter. The energy of the evolving state in eq 8 is $\hbar\omega(|\lambda|^2 + {}^1/_2)$, so we find that $|\lambda|^2 = E_{vib}/\hbar\omega$, where E_{vib} is the vibrational excitation energy in that particular mode. The probability of the fragment occupying an eigenstate $|n\rangle$ is

$$P_n = \frac{(E_{vib}/\hbar\omega)^n}{n!}e^{-E_{vib}/\hbar\omega} \qquad (9)$$

In Figure 9, we show the results for the vibrational probability up to $n = 5$ as a function of the center-of-mass scattering angle, averaged over all target orientations. The slowest trajectories contain the higher vibrational states, whereas the faster ones are mostly in the vibrational ground state in accordance with our previous discussion.

5. Conclusion

The simple END approach can qualitatively account for the observed time delay, both in the sense of lifetime of a short-lived three-particle complex and in the sense of velocity distribution. The differential cross section appears to be in good agreement with experiment and with full quantum calculations based on a single potential surface. There are still some questions about the results for the backward scattering, where the semclassical Schiff approximation does not introduce all of the needed quantum interference effects. The prediction of the different vibrational signatures of the forward- and backward-scattered products makes sense and should at least be qualitatively correct. The production of HD only for trajectories within an acceptance cone of 60° from the D−D bond axis is another interesting result. Differential cross sections are a rather severe

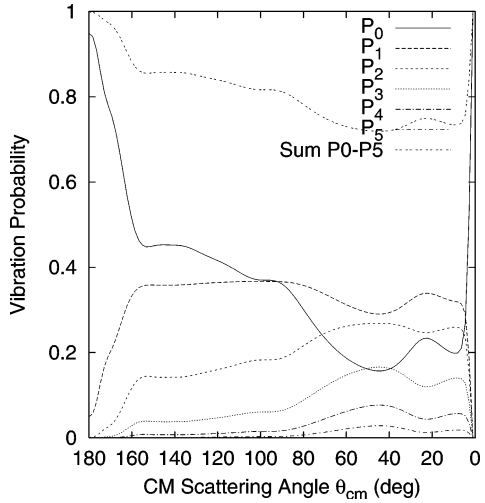

Figure 9. Probability (P_n) for HD to be found in various vibrational states (n) as a function of center-of-mass scattering angle in the collision $H + D_2 \rightarrow HD + D$.

test of theory and more applications of minimal END in this range of collision energies are needed. From past experience,[45] we know that integral cross sections with minimal END can be predicted with some confidence down to energies of the order of those considered here.

To bring this approach to applicability for lower energies and for neutral-on-neutral systems, one would argue that a better-correlated representation of the electrons is needed, and for hydrogenic systems, a quantum treatment of the nuclei would be necessary. Here, we have shown that, even in its minimal implementation, the END approach supports results obtained with full quantum treatments.

Acknowledgment. This work was supported partially by ONR (Grants N0014-97-1-0261 to Y.Ö. and E.D. and N0014-96-1-00707 to J.R.S.) and by an IBM SUR grant. This support is gratefully acknowledged.

References and Notes

(1) Levine, R. D.; Wu, S.-F. *Chem. Phys. Lett.* **1971**, *11*, 557.
(2) Truhlar, D. G.; Kuppermann, A. *J. Chem. Phys.* **1972**, *56*, 2232.
(3) Schatz, G. C.; Kuppermann, A. *J. Chem. Phys.* **1973**, *59*, 964.
(4) Schatz, G. D.; Kuppermann, A. *Phys. Rev. Lett.* **1975**, *35*, 1266.
(5) Nieh, J. C.; Valentini, J. J. *Phys. Rev. Lett.* **1989**, *60*, 519.
(6) Nieh, J. C.; Valentini, J. J. *J. Chem. Phys.* **1990**, *92*, 1083.
(7) Zhang, J.; Kouri, D. J.; Hang, K.; Sckwenke, D. W.; Truhlar, D. G. *J. Chem. Phys.* **1988**, *88*, 2492.
(8) Zhang, J. Z. H.; Miller, W. H. *Chem. Phys. Lett.* **1989**, *159*, 130.
(9) Kliner, D. A. V.; Adelman, D. E.; Zare, R. N. *J. Chem. Phys.* **1991**, *94*, 1069.
(10) Continetti, R. E.; Balko, B. A.; Lee, Y. *J. Chem. Phys.* **1990**, *93*, 5719.
(11) Miller, W. H.; Zhang, J. Z. H. *J. Phys. Chem.* **1991**, *95*, 12.
(12) Harich, S. A.; Dai, D. X.; Wang, C. C.; Yang, X. M.; Chao, S. D.; Skodje, R. T. *Nature* **2002**, *419*, 218.
(13) Schneider, L.; Seekamp-Rahn, K.; Borkowski, J.; Wrede, E.; Welge, K. H.; Aoiz, F. J.; Bañares, L.; D'Mello, M. J.; Herrero, V. J.; Saéz Rábanos, V.; Wyatt, R. E. *Science* **1995**, *269*, 207.
(14) Schneider, L.; Seekamp-Rahn, K.; Wrede, E.; Welge, K. H. *J. Chem. Phys.* **1997**, *107*, 6175.
(15) Xu, H.; Shafer-Ray, N. E.; Merkt, F.; Hughes, D. J.; Springer, M.; Tuckett, R. P.; Zare, R. N. *J. Chem. Phys.* **1995**, *103*, 5157.
(16) Fernández-Alonso, F.; Bean, B. D.; Zare, R. N. *J. Chem. Phys.* **1999**, *111*, 2490.
(17) Fernández-Alonso, F.; Bean, B. D.; Zare, R. N. *J. Chem. Phys.* **1999**, *111*, 1035.
(18) Fernández-Alonso, F.; Bean, B. D.; Zare, R. N. *J. Chem. Phys.* **1999**, *111*, 1022.
(19) Wrede, E.; Schneider, L.; Welge, K. H.; Aoiz, F. J.; Bañares, L.; Castillo, J. F.; Martínez-Haya, B.; Herrero, V. J. *J. Chem. Phys.* **1999**, *110*, 9971.
(20) Wrede, E.; Schneider, L. J. *Chem. Phys.* **1997**, *107*, 786.
(21) Kuppermannn, A.; Wu, Y. S. M. *Chem. Phys. Lett.* **1995**, *241*, 229.
(22) Kendrick, B. K.; Jayasinghe, L.; Moser, S.; Auzinsh, M.; Shafer-Ray, N. *Phys. Rev. Lett.* **2000**, *84*, 4325.
(23) Fernández-Alonso, F.; Bean, B. D.; Ayers, J. D.; Pomerantz, A. E.; Zare, R. N.; Bañares, L.; Aoiz, F. J. *Angew. Chem., Int. Ed.* **2000**, *39*, 2748.
(24) Boothroyd, A. I.; Keogh, W. J.; Martin, P. G.; Peterson, M. R. *J. Chem. Phys.* **1996**, *104*, 7139.
(25) Althorpe, S. A.; Fernández-Alonso, F.; Bean, B. D.; Ayers, J. D.; Pomerantz, A. E.; Zare, R. N.; Wrede, E. *Nature* **2002**, *416*, 67.
(26) Öhrn, Y.; Deumens, E.; Diz, A.; Longo, R.; Oreiro, J.; Taylor, H. In *Time-Dependent Quantum Molecular Dynamics*; Broeckhove, J., Lathouwers, L., Eds.; Plenum Press: New York, 1992; pp 279−292.
(27) Deumens, E. Diz, A.; Longo, R.; Öhrn, Y. *Rev. Mod. Phys.* **1994**, *66*, 917.
(28) Thouless, D. J. *Nucl. Phys.* **1960**, *21*, 225.
(29) Deumens, E.; Helgaker, T.; Diz, A.; Taylor, H.; Oreiro, J.; Mogensen, B.; Morales, J. A.; Coutinho-Neto, M.; Cabrera-Trujillo, R.; Jacquemin, D. *ENDyne Version 2.8 Software for Electron Nuclear Dynamics*; Quantum Theory Project, University of Florida: Gainesville, FL, 2000.
(30) Morales, J. A.; Diz, A. C.; Deumens, E.; Öhrn, Y. *J. Chem. Phys.* **1995**, *103*, 9968.
(31) Hedström, M.; Morales, J. A.; Deumens, E.; Öhrn, Y. *Chem. Phys. Lett.* **1997**, *279*, 241.
(32) Cabrera-Trujillo, R.; Sabin, J. R.; Öhrn, Y.; Deumens, E. *Phys. Rev. A* **2000**, *61*, 032719.
(33) Cabrera-Trujillo, R.; Sabin, J. R.; Öhrn, Y.; Deumens, E. *Phys. Rev. Lett.* **2000**, *84*, 5300.
(34) Cabrera-Trujillo, R.; Deumens, E.; Öhrn, Y.; Sabin, J. R. *Nucl. Instr. Methods* **2000**, *B168*, 484.
(35) Cabrera-Trujillo, R.; Sabin, J. R.; Deumens, E.; Öhrn, Y. In *Application of Accelerators in Research and Industry, Sixteenth International Conference*; Duggan, J. L., Morgan, I. L., Eds.; American Institute of Physics: New York, p 3.
(36) Cabrera-Trujillo, R.; Öhrn, Y.; Sabin, J. R.; Deumens, E. *Phys. Rev. A.* **2002**, *65*, 024901.
(37) Coutinho-Neto, M.; Deumens, E.; Öhrn, Y. *J. Chem. Phys.* **2002**, *116*, 2794.
(38) Dunning, T. H. *J. Chem. Phys*. **1989**, *90*, 1007.
(39) Woon, D. E.; Dunning, T. H. *J. Chem. Phys.* **1994**, *100*, 2975.
(40) Jacquemin, D.; Morales, J. A.; Deumens, E.; Öhrn, Y. *J. Chem. Phys.* **1997**, *107*, 6146.
(41) Schiff, L. I. *Phys. Rev.* **1956**, *103*, 443.
(42) Kitsopoulos, T. N.; Buntine, M. A.; Baldwin, D. P.; Zare, R. N.; Chandler, D. W. *Science* **1993**, *260*, 1605.
(43) Wrede, E.; Schnieder, L. *J. Chem. Phys.* **1997**, *107*, 786.
(44) Blass, A.; Deumens, E.; Öhrn, Y. *J. Chem. Phys.* **2001**, *115*, 8366.
(45) Öhrn, Y.; Oreiro, J.; Deumens, E. *Int. J. Quantum Chem.* **1996**, *58*, 583.